

Model of semiconductor converters for the simulation of an asymmetric loads in an autonomous power supply system

Saidjon Tavarov¹, Mihail Senyuk², Murodbek Safaraliev², Sergey Kokin², Alexander Tavlintsev²,
Andrey Svyatykh³

¹Institute of Engineering and Technology, South Ural State University, Chelybinsk, Russia

²Department of Automated Electrical Systems, Ural Federal University, Yekaterinburg, Russia

³Uralenergosbyt LLC, Chelybinsk, Russia

Article Info

Article history:

Received Feb 16, 2024

Revised Oct 10, 2024

Accepted Nov 20, 2024

Keywords:

Asymmetry

Load

Model

Semiconductor converter

Voltage

ABSTRACT

This article is devoted to the development of computer model with semiconductor converters for the simulation of asymmetric loads allowing to solve the voltage symmetry problems under asymmetric loads (active and active-inductive) for isolated electric networks with renewable energy sources (mini hydroelectric power plants). A model of a symmetry device has been developed in the MATLAB/Simulink environment based on a proportional-integral controller and a relay controller - P. The effectiveness of their use depends on the load's nature. The implementation of a voltage converter is presented considering a three-phase inverter with discrete key switching at 120, 150, and 180 degrees with a purely active load. Based on the harmonic analysis of the three-phase voltage at discrete conversion, the value of the first harmonic is determined. Voltage transformations under active-inductive load at 120, 150, and 180 degrees are mathematically described. To determine the harmonic spectrum, an analysis of the fast Fourier transform for the three-phase voltage of a MATLAB/Simulink semiconductor converter was carried out. It is established that the alternating current output voltage is generated on the output side of the inverter of a three-phase voltage source through a three-phase load connected by a star with a harmonic suppression method.

This is an open access article under the [CC BY-SA](https://creativecommons.org/licenses/by-sa/4.0/) license.



Corresponding Author:

Murodbek Safaraliev

Department of Automated Electrical Systems, Ural Federal University

620002 Yekaterinburg, Russia

Email: murodbek_03@mail.ru

1. INTRODUCTION

Due to the increasing range of single-phase electric receivers, interest in the proposed methods of monitoring and controlling converters is sharply increasing. These electric receivers create asymmetric modes in a three-phase four-wire power supply system when consumed, which leads to the appearance of current in a zero conductor. Consequently, four-wire converters proposed by many authors [1]–[10] will be effectively used to control a semiconductor converter in such modes. At the same time, it should be noted that this system has so far found wide application only in autonomous power supply systems. This is primarily due to the simplification of the control and management system. This control method is based on transforming the coordinate system from a three-phase to a two-phase one, followed by an inverse transformation [11]–[20]. At the same time, for the successful implementation of the conversion, not only information about instantaneous voltage values is needed, but also about instantaneous current values [21]–[30]. A diagram of the implementation of a control system with data on voltages and currents is shown

in [29], [30] (This scheme forms a rotating voltage vector corresponding to the symmetric mode using a phase-locked loop (PLL) converter. Based on information about the angular position of the voltage vector (angle Θ), three-phase currents and voltages are converted into two-phase ones in a rotating coordinate system. Next, the two-phase voltage system is balanced using proportional-integral (PI) regulators and the reverse voltage conversion is carried out, from two-phase to three-phase).

Various current regulators are offered for the voltage source inverter: linear and nonlinear [31]–[35]. A linear current regulator requires knowledge of all load parameters and includes a PI regulator, a state feedback regulator, and a predictive current regulator. The nonlinear controller provides a good dynamic response of the control system, while it does not require load information. This controller includes hysteresis control, linear type control, and delta modulator [36].

Obtaining alternating current (AC) output signals from direct current (DC) power sources is the main task of power electronics converters [36], [37]. Controlled AC power waveforms are needed in many applications. These different applications can be classified based on the controlled AC parameters, which are the magnitude, frequency, and phase angle of the AC output waveform, and the type of AC output being controlled. The AC output waveform will take discrete values such that the fundamental component appears as a sinusoidal signal, even though the modulated output signal is not sinusoidal.

Key characteristics of the current regulator:

- “Extremely good dynamics”
- Instantaneous monitoring of load current with high (good) accuracy
- Overcurrent protection
- Over-current deviation
- Error compensation when changing load parameters
- Error compensation for parameter sensitivity
- Maintaining constant voltage in the DC and AC link [38].

In study [36], a control device with a delta modulator at zero hysteresis and a modified linear type current regulator for a voltage source inverter are considered. The two regulators were compared in MATLAB for different values of load parameters as shown in Table 1.

Table 1. Comparison of current regulators

Name of the parameters	Modified linear type current regulator	Delta Modulator
Dynamic characteristics	“Good ones”	“Good ones”
Current ripple	Big	Smaller
The coefficient of nonlinear distortion of the load current	Smaller	Big
Limiting the switching frequency	Carrier frequency limitation	Fixed at the cutoff frequency the integrator

In [39], a computer model of an AC electric drive with a multi-level voltage inverter with frequency converters developed in MATLAB was described (MVIIF). The studied electric drive circuit was a 13-level MVIIF, consisting of 18 symmetrical inverter cells, and an asynchronous motor ($P_n = 8 \text{ MW}$, $U = 10 \text{ kV}$). The control system model MATLAB-based included 2 subsystem units: a speed controller unit and an inverter control system unit. The speed controller was a PI controller. The result of the work was the efficiency calculation method implemented in MATLAB, which takes into account dynamic losses in semiconductor devices. In [40], the PI controller is described in more detail, and the behavior of the drive system is compared with hybrid fuzzy PI, conventional PI and fuzzy controllers, genetic algorithm based proportional-integral (GA-PI) and adaptive network-based fuzzy inference system (ANFIS) torque and speed controllers. Due to changes in engine parameters when its operating mode is disturbed, the PI controller requires precise adjustment of the proportional gain and the integral time constant, but this is difficult to achieve, this problem is overcome by developing regulators with fuzzy logic [41], but the performance of such a regulator surpasses the PI controller only in transient conditions. In [42] (4 of 7), an improvement of the PI controller based on a fuzzy control model was proposed, but it is necessary to manually determine the limits of the gain coefficients. The hybrid fuzzy-PI (fuzzy PI) controller works as a PI controller in steady-state modes, and as a fuzzy controller only during overspeed or under-speed [43] (5 of 7). However, both regulators have disadvantages that can be eliminated by expanding their functions. To ensure independent operation, the PI controller must be able to adapt to changes in the dynamic characteristics of the installation. The genetic algorithm (GA) allows you to search for optimal parameters of the regulator.

The main disadvantage of fuzzy control is the lack of well-established design and configuration techniques [44], [45]. The selection of an appropriate rule base, depending on the situation, can be achieved

by using the ANFIS regulator. According to the simulation results, the ANFIS regulator provides the greatest dynamic response and generally works better than other regulators [46]. Studies using traditional control methods with the addition of a PI regulator were also described in [47]. Among the traditional methods, the following were considered: a current regulator with hysteresis and a linear change comparison current regulator. The PI controller made it possible to improve existing methods, to suppress higher harmonics, torque pulsations, noise, and electromagnetic interference. The modified methods allowed the stator current forms to become smoother. According to the research results, a current regulator with hysteresis and a PI current regulator turned out to be more efficient than a regulator built based on comparing the linear change of current with a PI regulator.

Current regulators with pulse width modulation (PWM) are considered in modern studies [39], [48]. PWM-controlled inverters have a significant advantage [39], [48] and as a result, are widely used in AC drives. In the article [39], the performance of a hysteresis current regulator and a PI current regulator using PWM technology for a voltage source inverter was tested. The simulation results of the current regulators showed that both regulators can provide the necessary regulation of the output current. For digital control, the most common PWM method is the sinusoidal PWM (SPWM) method, because it has lower power losses, fewer harmonics, and can be easily implemented [47]. In this work, a simple model was presented with the implementation of digital signal processing (DSP) based on the TMS320F28335 chip for a three-phase voltage source inverter (VSI) using sinusoidal pulse width modulation (SPWM) technology, implemented using MATLAB R2019a. The simulation result was tested experimentally on a three-phase voltage source inverter VSI training model and showed that the simulation was performed fairly accurately, while the implementation of this device is simple

The frequency converter and the motor are not always close enough, in the electric drive system of various industries, the distance between them can reach hundreds or thousands of meters, *i.e.* the converter must be connected using a long cable [49]. To suppress the effect of overvoltage on the motor side, the article [50] describes several methods for solving the problem in an overview, as well as a new method for suppressing resonant overvoltage of a drive system with a long cable, considering the variable frequency of current and voltage. Based on the mathematical model, an improved constant active power controller was developed. According to the results of the study, the algorithm has high control efficiency and good reliability in controlling the phenomenon of resonant overvoltage and can effectively ensure the safety of operation of a drive with a frequency converter and a long cable.

2. METHOD

The schemes of DC-to-AC converters that have found the greatest application by forming a sinusoidal three-phase voltage when solving problems of regulating the effective voltage value at a fixed frequency most often turn out to be difficult to implement and practically cannot maintain operability with single failures. Solving the problem of voltage symmetry by traditional methods dramatically complicates the circuit and algorithms of the converter, therefore they need to be improved together with algorithms for generating alternating voltage. With an increase in the number of phases, the necessary energy indicators are achieved by using a generator with a closed winding, while it is necessary to consider that in cases of damage to one of the windings or the rectifier key, its operating mode is not disrupted. This is explained by the fact that during the switching process the combination and number of phases connected to the positive and negative buses of the power source changes. In this regard, in the case of an asymmetric load, these parameters are different at each cycle and, with six-cycle switching of the inverter, are repeated every five cycles.

2.1. Simulation of an inverter as a voltage source using discrete switching with a PI controller

Let's consider the simulation of voltage converters with discrete switching based on a three-phase inverter feeding a symmetrical and unbalanced load. The inverter of the three-phase voltage source will be modeled in the MATLAB/Simulink environment. Figure 1 shows a model of a symmetry device (SD) based on a PI controller implemented in MATLAB/Simulink, forming a set value of the voltage at a common point (CP), and a control unit for additional transistors (SD) is shown in Figure 1.

The discrete signal controlling the operation of the inverter is implemented by the control unit (block parameters: pulse generator) in the MATLAB/Simulink environment and comes to each of the six transistors. To obtain a three-phase output voltage, the six switches must be controlled so that the output waveform is close to sinusoidal. To clarify this, a star-connected resistive load is connected to the inverter shown in Figure 1.

The correctness of the model under symmetrical load with the waveforms of the phase voltage of the inverter is shown in Figures 2 to 4. For the 120° mode of the three-phase voltage inverter, each of the

semiconductor switches conducts 120° of the cycle. As in the 180° mode, the inverter in 120° mode also requires six steps of 60° each to complete one cycle of the AC output voltage. In the 150° switching mode, each inverter switch conducts on an interval of 150° degrees. It has twelve steps, each of which has a duration of 30° degrees to complete one cycle of the output AC voltage. Three transistors conduct in one interval, as in the 180° mode, while only two transistors conduct in the next interval, as in the 120° mode. The stability of maintaining the output parameters of a three-phase voltage inverter under an unbalanced load is carried out using a block forming a set voltage value (CP) in Figure 5. In this unit, an additional transistor is controlled, which generates a reference signal of a set value of the common point voltage Figure 6.

To achieve a reference signal, the voltage at an unbalanced load at the output of a three-phase inverter and the voltage at a common point relative to the minus bus changes its value and when comparing the reference signal with the signal at a common point relative to the minus bus, the regulator acts on the control unit of additional transistors in Figure 7 (in Figure 1, the block of the symmetry device is highlighted in red). However, the SD based on the PI controller operates under active load and depends on the voltage and current in the zero wire. When an inductive load appears, the control device is too late. In this case, it is necessary to use a device with discrete switching and a P-regulator as shown in Figure 8.

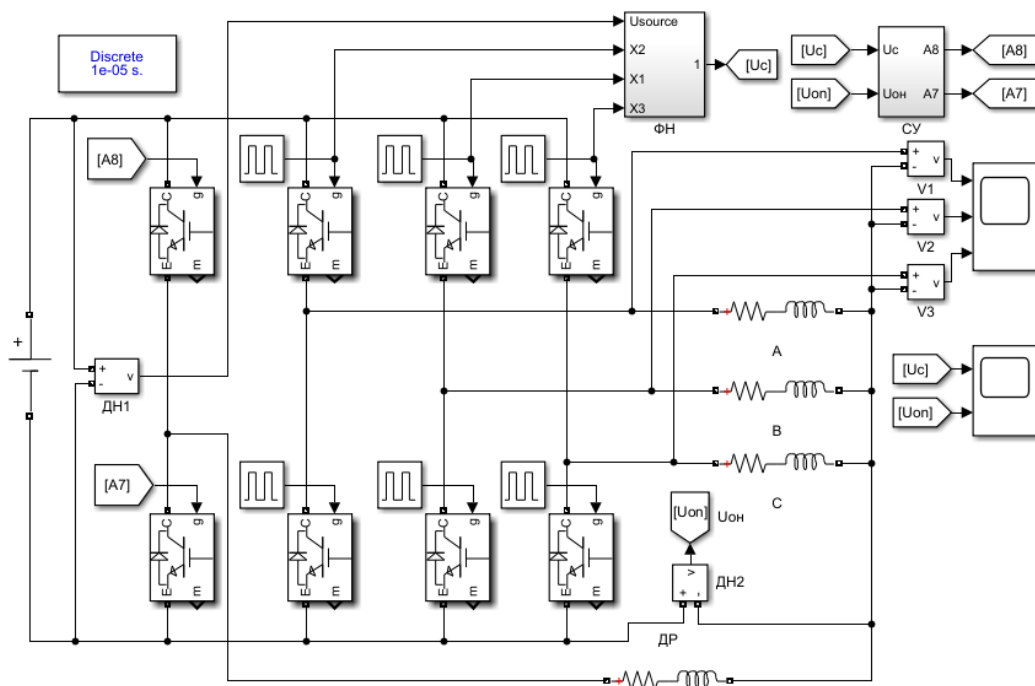


Figure 1. A model of the SD symmetry device based on a PI controller in MATLAB/Simulink

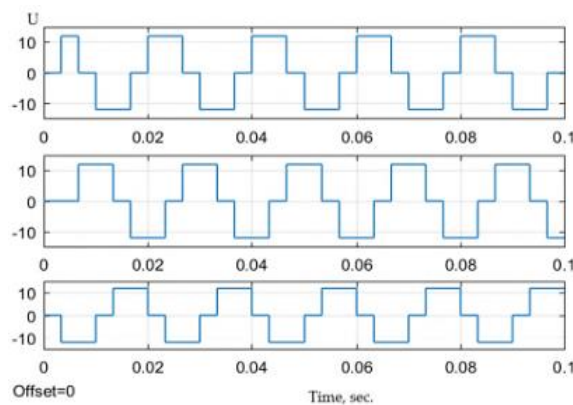


Figure 2. The waveform of the phase voltage at 120-degree switching

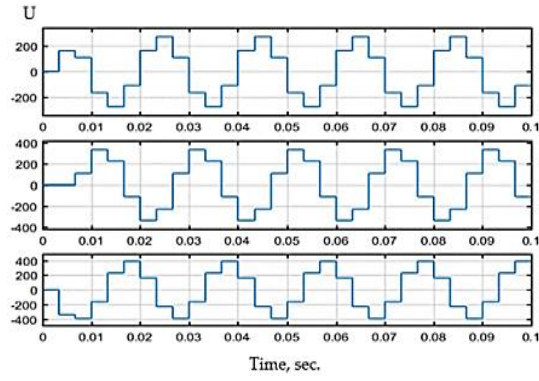


Figure 3. The waveform of the phase voltage at 150-degree switching

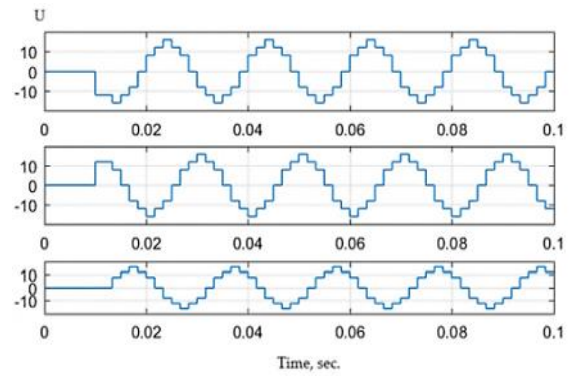


Figure 4. The waveform of the phase voltage at 180-degree switching

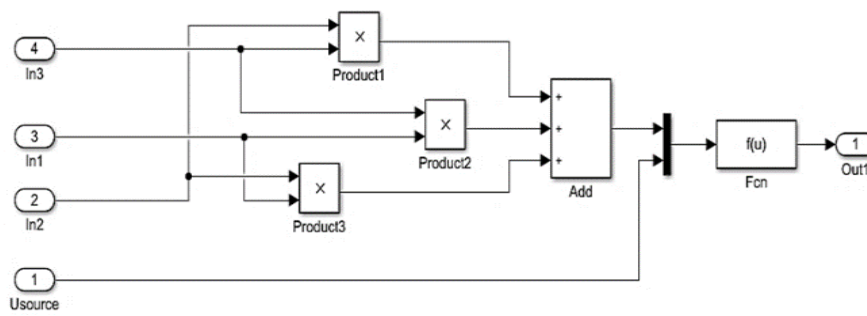


Figure 5. A common point voltage setpoint shaper

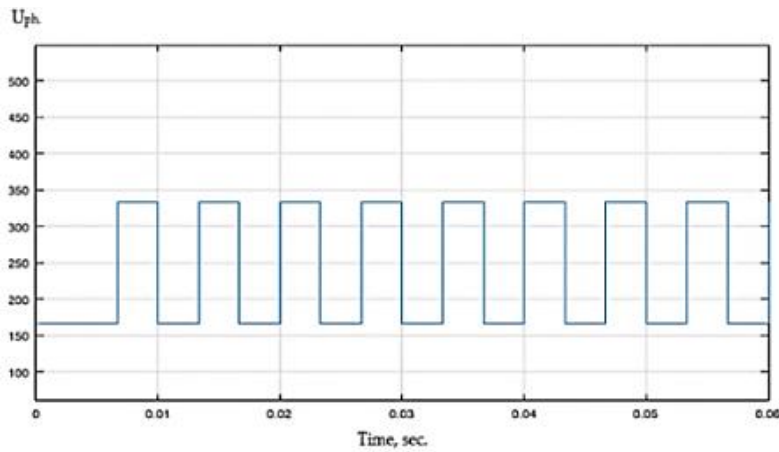


Figure 6. The reference voltage signal at the common point

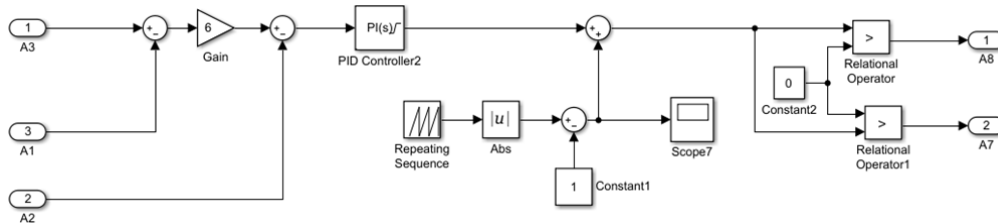


Figure 7. A symmetrical device based on a PI controller

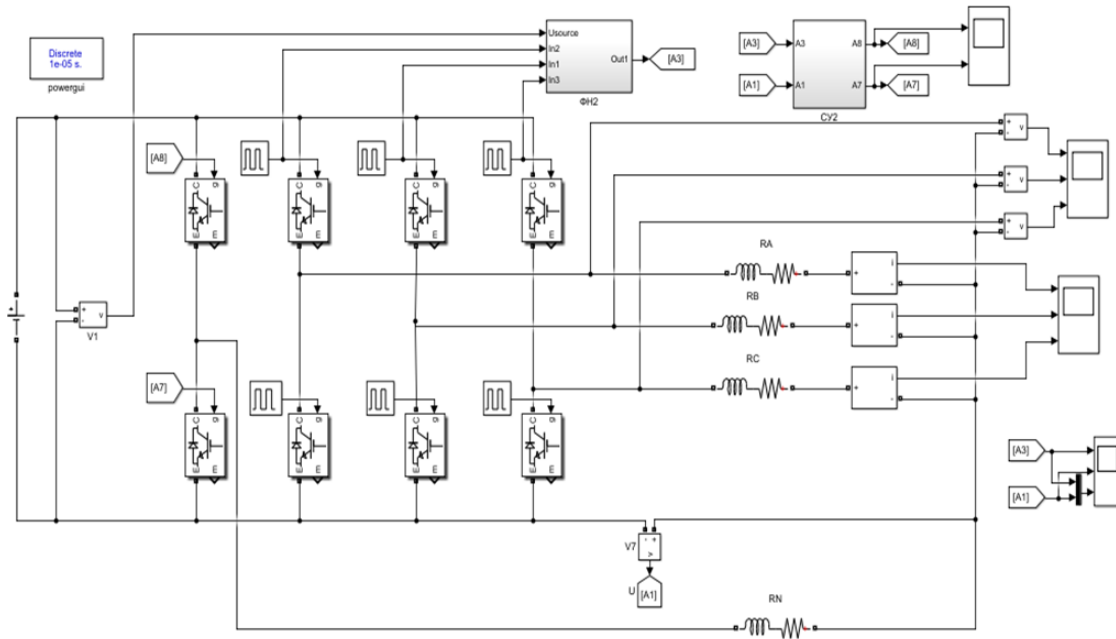


Figure 8. A model of a symmetry device (SD) based on a P-regulator in MATLAB/Simulink

2.2. Implementation of a voltage converter based on a three-phase inverter with discrete key switching

The use of discrete switching of inverter power keys for converting direct voltage into alternating voltage, even in the simplest case with 180-degree six-cycle switching, allows obtaining a phase voltage at the inverter output with a content of higher harmonics of no more than 4.5% of the effective value of the total voltage. In this case, six insulated gate bipolar transistor (IGBT) transistors are required, as shown in Figure 1. With an active-inductive symmetrical phase load in the case of discrete switching, the shape of the output voltages remains the same as with a purely active load. In the case of an asymmetry of phase loads, the shape of the phase voltages is distorted [10]. Therefore, the voltage on the parallel resistors is equal to $U_s/3$, and on the series resistor - $2/3U_s$ [10]. It is assumed that a purely active load is connected to the converter: $R_A = R_B = R_C = 10 \text{ Ohm}$ [10].

The discrete values generated by the inverter impose additional restrictions on some applications. For example, sensitive loads cannot be connected directly to the inverter output. The quality of the output signals must be improved with harmonic filters to meet the required quality standards. In addition, capacitive loads will increase the influence of the discrete output voltage by adding more current peaks [10]. To obtain a three-phase output voltage, the six switches must be controlled in such a way that the output waveform is close to sinusoidal. To clarify this, a resistive load connected in a star is connected to the inverter shown in Figure 4. In cases where there are no strict requirements for the content of higher harmonics in the supply voltage, a simple converter with discrete commutation can be used: i) Each inverter switch is open at an interval of 120° ; ii) Each inverter switch is open at an interval of 150° ; and iii) Each inverter key is open at 180° interval.

For the 120° mode of the three-phase voltage inverter, each of the semiconductor switches conducts for 120° of the cycle. As in the 180° mode, the inverter in the 120° mode also requires six steps of 60° each to complete one cycle of the AC output voltage. Table 2 shows the conducting transistors during each individual interval.

In a three-phase inverter, each switch conducts 180° of the cycle, a pair of semiconductor keys in each arm, *i.e.* VT1, VT4; VT3, VT6 and VT5, VT2 are switched on with a time interval of 180° . This is also proven by the lower group of switches. Table 3 shows the conducting transistors during each individual interval [10].

In the 150° switching mode, each inverter switch conducts over an interval of 150° degrees. It has twelve steps, each of which has a duration of 30° degrees to complete one cycle of the output AC voltage. Three transistors conduct in one interval, as in the 180° mode, while only two transistors conduct in the next interval, as in the 120° mode. Table 4 shows the conducting transistors during each individual interval [10].

Table 2. Operation in 120° commutation mode

No.	Interval	Key (on)	Polarity		
			(A)	(B)	(C)
1	0-60	VT1, VT6	+	0	-
2	60-120	VT3, VT6	0	+	-
3	120-180	VT3, VT2	-	+	0
4	180,240	VT5, VT2	-	0	+
5	240-300	VT5, VT4	0	-	+
6	300-360	VT1, VT6	+	-	0

Table 3. Operation in 180° commutation mode

No.	Interval	Key (on)	Polarity		
			(A)	(B)	(C)
1	0-60	VT1, VT5, VT6	+	-	+
2	60-120	VT2, VT6, VT1	+	-	-
3	120-180	VT3, VT1, VT2	+	+	-
4	180,240	VT4, VT2, VT3	-	+	-
5	240-300	VT3, VT4, VT5	-	+	+
6	300-360	VT4, VT5, VT6	-	-	+

Table 4. Operation in 150° commutation mode

No.	Interval	Key (on)	Polarity		
			(A)	(B)	(C)
1	0-60	VT1, VT2, VT6	+	-	-
2	60-120	VT1, VT2	+	0	-
3	120-180	VT1, VT2, VT3	+	+	-
4	180-240	VT2, VT3	0	+	-
5	240-300	VT2, VT3, VT4	-	+	-
6	300-360	VT3, VT4	-	+	0
7	360-420	VT3, VT4, VT5	-	+	+
8	420-480	VT4, VT5	-	0	+
9	480-540	VT4, VT5, VT6	-	-	+
10	540-600	VT5, VT6	0	-	+
11	600-660	VT1, VT5, VT6	+	-	+
12	660-720	VT1, VT6	+	-	0

2.3. Harmonic analysis of three-phase voltage with discrete conversion

For high efficiency of DC-to-AC conversion and peak power tracking, the inverter must have low harmonic distortion along with low electromagnetic interference and high-power factor. In order to suppress harmonics and control unbalanced loads, there are several switching methods for inverter control [1]–[9]. The discrete control method of power keys is one of them [10]–[30]. The performance of a discrete switching circuit can be estimated based on the analysis of the distortion level at the inverter output, the spectrum of harmonics contained in this voltage and the complexity of the implementation. According to [11]–[15], based on the obtained timing diagrams, we calculate the effective values of the phase voltages [16]–[22].

This diagram shows that the output voltage between the lines is $+U_s$, 0 or $-U_s$. The instantaneous interfacial voltage U_{ab} can be expressed in a Fourier series, as described in:

$$U_{ab} = \sum_{n=1,3,5}^{\infty} \frac{4U_s}{n\pi} \cdot \cos\left(\frac{n\pi}{6}\right) \cdot \sin\left(n\left(\omega t + \frac{\pi}{6}\right)\right) \quad (1)$$

Then U_{bc} and U_{ca} shifting U_{ab} on 120° and 240° we get,

$$U_{bc} = \sum_{n=1,3,5}^{\infty} \frac{4U_s}{n\pi} \cdot \cos\left(\frac{n\pi}{6}\right) \cdot \sin\left(n\left(\omega t - \frac{\pi}{2}\right)\right), \quad (2)$$

$$U_{ca} = \sum_{n=1,3,5}^{\infty} \frac{4U_s}{n\pi} \cdot \cos\left(\frac{n\pi}{6}\right) \cdot \sin n\left(\omega t - \frac{7\pi}{6}\right). \quad (3)$$

It is also shown that in (1), (2), and (3) the harmonics of the triplets are zero in linear voltage. The rated maximum sinusoidal (RMS) voltage between the lines is expressed in (4), whereas the RMS voltage between the lines and the neutral is in (5):

$$U_L = \sqrt{\left[\frac{2}{2\pi} \int_0^{2\pi} U_s^2 d\omega t\right]} = \sqrt{\frac{2}{3}} U_s, \quad (4)$$

$$U_{cal.} = \frac{U_L}{\sqrt{3}}. \quad (5)$$

The use of discrete switching of inverter power keys for converting direct voltage into alternating voltage, even in the simplest case with 180° six-cycle switching, allows obtaining a phase voltage at the inverter output with a content of higher harmonics of no more than 4.5% of the effective value of the total voltage.

2.4. Mathematical description of voltage conversion under active-inductive load

Now let us estimate the influence of inductance on the voltage diagram on the neutral wire with an active-inductive load. Let us consider the case of 180-degree switching as the most easily implemented and quite effective from the point of view of the content of higher harmonics in the phase voltages. As was shown [11], in this case for the symmetrical mode and active load of the converter we have the form of phase voltages (U_a, U_b, U_c), and the zero point voltage relative to the minus bus of the power source (U_0), corresponding to Figure 1. In Figure 9, the angular interval is plotted along the abscissa axis, and the relative voltage value as a fraction of the DC source voltage is plotted along the ordinate axis. Obviously, the task of symmetrization is to ensure that the voltage waveform shown in Figure 9 is preserved or brought closer to it with any difference and any type of phase load resistance.

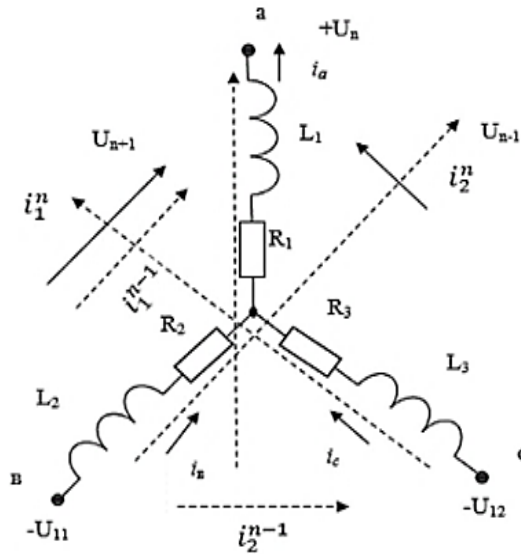


Figure 9. Connection diagram of the phase loads of the converter to a DC source

In the case of a symmetrical active-inductive load ($R_1 = R_2 = R_3 = R, L_1 = L_2 = L_3 = L$), on one switching cycle, the circuit for connecting the winding through the inverter switches to a DC source. The dotted arrow with the designation shows the direction of the voltage vector at the considered, previous, and subsequent switching interval of the converter keys in Figure 9. Solid arrows indicate currents i_1 and i_2 at the media control interface (MCI) in question, and dotted ones indicate the same currents at the previous media control (MC) AND. To describe electromagnetic processes, we will draw up voltage equations to determine the contour currents i_1 and i_2 , neglecting the mutual inductances and capacitances of phase loads, which we will take into account later:

$$U = 2(LP + R)i_1 + (LP + R)i_2, \tag{6}$$

where \bar{i}_1, \bar{i}_2 is the differentiation operator, U is the voltage of the DC source, and R is the relative value of the current.

Moving on to relative units, we get:

$$\begin{aligned} 1 &= \bar{i}_1(1 + \rho\tau), \\ 1 &= \bar{i}_2(1 + \rho\tau), \end{aligned} \tag{7}$$

where: $\rho\tau$ – is the electromagnetic time constant of the winding.

In the future, the dashes denoting relative units will be omitted. Then the solution of the voltage equations of the current circuits will be written as (8).

$$\begin{aligned} i_1(t) &= (1 - e^{-\frac{t}{\tau}}) + i_{10}e^{-\frac{t}{\tau}}, \\ i_2(t) &= (1 - e^{-\frac{t}{\tau}}) + i_{20}e^{-\frac{t}{\tau}}, \end{aligned} \tag{8}$$

where i_{10} and i_{20} are the initial values of the contour currents in the considered n th interval, equal to the final values of similar currents in the previous $n-1$ interval.

According to Figure 9, you can write as (9).

$$\begin{aligned} i_{10}^n &= i_{ck}^{n-1} = i_{1k}^{n-1} + i_{2k}^{n-1}, \\ i_{20}^n &= -i_{ck}^{n-1} = -i_{2k}^{n-1}. \end{aligned} \quad (9)$$

where the upper index indicates the switching cycle, and the lower one indicates the name of the phase with the final value of the current in it.

In turn, the final values of the currents on the MC are determined from (7) for a time equal to the duration of the MCI. Solving (8) and (9) together when $t = T_k$, where T_k – the duration of the MCI, for a steady-state operation mode, we get:

$$\begin{aligned} i_{10} &= \frac{(1-b)+(1-b)(1-b)}{1-b+b^2}, \\ i_{20} &= \frac{(1-b)+(1-b)(1-b)b}{1-b+b^2}. \end{aligned} \quad (10)$$

where $b = e^{-\frac{T_k}{\tau}}$.

Substituting the initial values of the currents obtained in (7), we can find the law of change of contour currents on the MCI for the steady-state operation mode. Knowing the law of change of contour currents, we can find the law of change of phase currents:

$$i_a = i_1 + i_2; \quad i_b = -i_1; \quad i_c = -i_2, \quad (11)$$

$$U_{ph} = \frac{1}{3} i_{ph}^{(t)} (1 + \tau\rho). \quad (12)$$

Using the phase voltage (12), we can find the law of change in phase voltages at microcontroller (MK). The coefficient $1/3$ takes into account that the base resistance, according to (7), is three times greater than the phase resistance. Therefore, we can make sure that the phase voltages at a symmetrical active-inductive load change in steady state.

This can be seen by taking the duration of the MCI long enough for the current in the winding to reach a steady value at the end of this interval. To do this, in the resulting equations, it is enough to take $b = 0$. From here we get $i_{10} = 2$, $i_{20} = -1$, and the equations of contour currents will look like:

$$\begin{aligned} i_1(t) &= (1 - e^{-\frac{t}{\tau}}) + 2e^{-\frac{t}{\tau}}, \\ i_2(t) &= (1 - e^{-\frac{t}{\tau}}) + e^{-\frac{t}{\tau}}. \end{aligned} \quad (13)$$

Then according to (11) and (13) we get (14):

$$i_a(t) = i_1(t) + i_2(t) = 2 - e^{-\frac{t}{\tau}}. \quad (14)$$

Substituting $i_{a(t)}$ from (14) into (12) and differentiating, we get $U_a(t) = 2/3$. Thus, the presence of inductance in the load in a symmetrical mode does not distort the phase voltage diagram. Physically, this is explained by the fact that the electromagnetic processes of current rise in the connected phase and current decrease in the disconnected phase occur at the same speed, determined by the electromagnetic constant τ .

In the case of an asymmetric inductively active load, each phase will have its constant value. It will lead to an asymmetry of phase voltages not only due to the difference in active loads but also due to the difference in the rate of flow of electromagnetic processes of the phases being switched on and off. The diagram of phase voltages and zero point voltages relative to the “minus” bus in some particular case will look like, as shown in Figure 10 (solid lines).

To solve the issues of output voltage symmetrization, the following principle is shown in Figure 11. The original replacement circuit without symmetrization is shown in Figure 11(a). Using the additional resistance in Figure 11(b), the control key G8 is replaced or the current is reduced at the star's midpoint, so that in this case the voltage drop across the resistance R_2 is equal to $2/3U_s$.

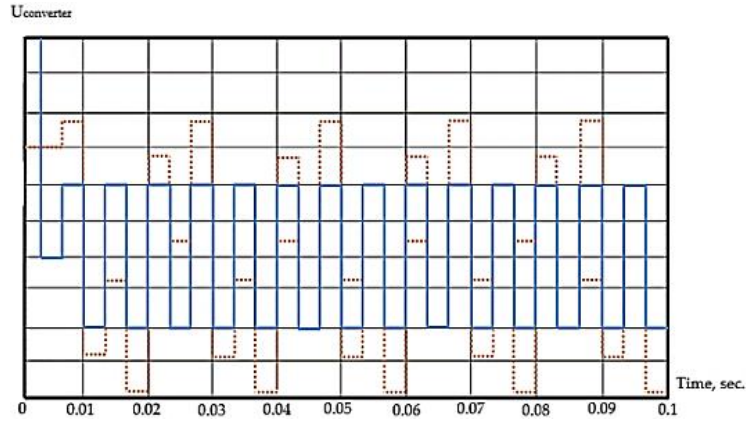


Figure 10. Zero-point voltage of the power supply in symmetrical (solid lines) and asymmetrical (dashed lines) modes

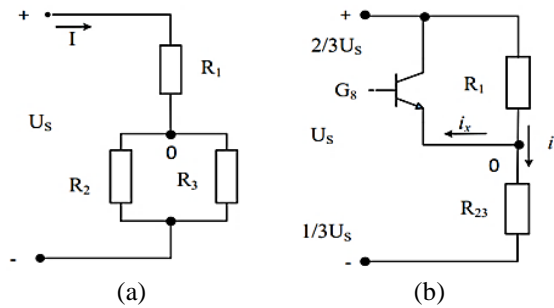


Figure 11. Output voltage symmetrization: (a) the original substitution scheme without symmetry and (b) the equivalent substitution scheme with symmetry

The required current value is determined by (15):

$$i_{id} = \frac{\left(\frac{2}{3}U_d\right)U_{R_2}}{R_2}, \tag{15}$$

where U_{R_2} – the existing phase voltage on the resistor R_2 ;

$$U_{R_2} = i_1 \cdot R_2, \tag{16}$$

i_1 – current consumed from the network;

$$i_1 = \frac{U_d}{U_{equ}}$$

where

$$U_{equ} = \frac{R_1 \cdot R_2}{R_1 + R_2} \tag{17}$$

Now, knowing i_{id} the adjusted phase voltage can be calculated:

$$U_{R_2} = (i_1 + i_{is}) R_2 \tag{18}$$

After calculation, we obtain a time diagram of the symmetry current in Figure 12, and the time diagram of phase voltages will have the same appearance as with a symmetrical load, as shown in Figure 1. Figure 13 shows the transient process of the automatic voltage balancing system at a certain value of the k coefficient.

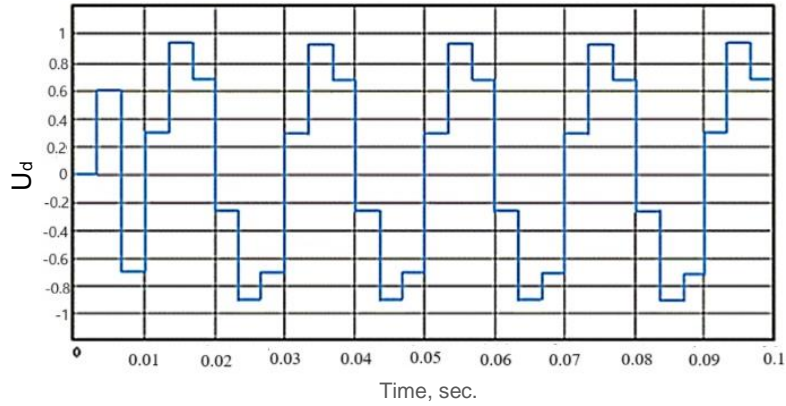


Figure 12. The current of symmetry

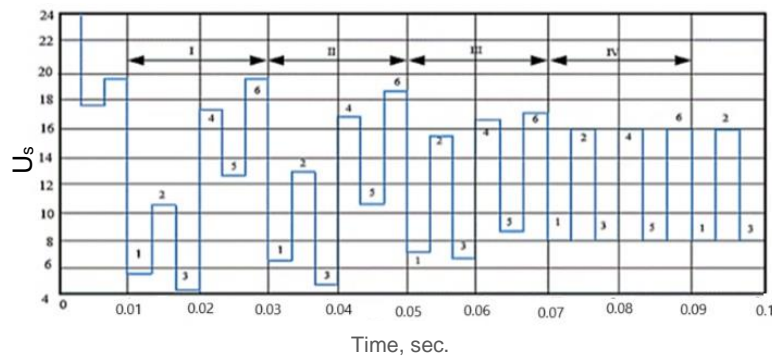


Figure 13. Diagram explaining the principle of operation of the current regulator: I, II, III and IV—the period of the fundamental frequency, 1, 2, 3, 4, 5, and 6 is the clock number of the discrete switching within the period

The first period is without a regulator, and in the third, fourth and fifth periods the current compensation regulator operates, and in three periods the zero point voltage has become symmetrical. It is obvious that the appearance of reactive elements in the inverter load will lead to a change in the voltage shape at the network zero point, since the shape of the phase currents can differ significantly from the shape of the voltages. However, the most important indicator remains the equality of the voltage amplitude at the zero point, and it is according to this criterion that the keys of the fourth additional inverter rack should be controlled Figure 12.

The algorithm for controlling the keys of the fourth rack will not change when implementing different control methods: discrete, PWM modulation, vector control and with different degree switching [10].

$$\begin{aligned} I_{k_1}[n] &= I_k[n-1] + \Delta U[n-1] \cdot k, \\ I_{k_2}[n] &= I_k[n-1] + \Delta U[n-1] \cdot k, \end{aligned} \tag{19}$$

where $I_k[n]$, $I_k[n-1]$ – compensating current of the corresponding key on the n th and previous control cycles, ΔU – the deviation of the voltage of the common point from the set one:

$$\Delta U = U_{oc} - U_{oph} \tag{20}$$

where U_{oc} – the set voltage of the common point relative to the bus “–” in symmetrical operation mode can take the value $+1/3U_s$ on clock cycles No. 2-4-6 and $+2/3U_s$ on clock cycles No. 1-3-5, U_{oph} – the actual voltage of the common point.

The first period is without a regulator, and in the third, fourth, and fifth periods the current compensation regulator is working, and in three periods the zero-point voltage has become symmetrical. The

appearance of reactive elements in the inverter load will lead to a change in the voltage shape at the zero point of the network, since the shape of the phase currents may differ significantly from the shape of the voltages. However, the most important indicator remains the equality of the voltage amplitude at the zero point, and it is according to this criterion that the keys of the fourth additional inverter rack should be controlled. The key management algorithm of the fourth rack will not change when implementing different control methods: discrete, PWM modulation, vector control, and at different degree switching. However, difficulties may arise if we provide sinusoidal currents by the method of space-vector modulation at a relatively low frequency or when connecting an inductive load. Here there is a problem of filtering voltages at the zero point, which can cause a delay in the formation of control signals and, as a result, a loss of stability of the regulator.

To equalize the rate of electromagnetic processes and at the same time to balance the voltages from the difference in active resistances, it is advisable to connect the common point (zero) of the three-phase network to an additional rack of a three-phase bridge inverter (keys G7, G8), as shown in Figure 11. The keys of the additional rack can be controlled from a relay controller (P) assembled by the diagram Figure 10. If we take the voltage difference at the zero point at a symmetrical load (U_{0c}) and the actual unbalanced load (U_{0z}) as the input voltage for the relay element, and the output signals (X_{c1}, X_{c2}) are formed according to the law:

$$\begin{aligned} x_{c1} = 1, x_{c2} = 0 &\rightarrow U_{0c} - U_{0z} > |\delta U|, \\ x_{c1} = 1, x_{c2} = 1 &\rightarrow U_{0c} - U_{0z} < -|\delta U|, \\ x_{c1} = 1, x_{c2} = 0 &\rightarrow |U_{0c} - U_{0z}| \leq |\delta U|, \end{aligned} \quad (21)$$

where δU – the dead zone of the relay, then the potential of the zero point will be continuously pulled up to the potential corresponding to the symmetrical load. Therefore, the symmetry of the phase voltages will be ensured. The switching frequency of the relay element will be determined by the time constant of the phase load. In the case of a purely active load of the converter, it will tend to infinity. To limit it, a throttle must be inserted into the zero wire. In addition, to limit the switching frequency of the relay, it may be necessary to introduce hysteresis into the control algorithm.

3. RESULTS AND DISCUSSION

The AC output voltage is generated on the output side of the inverter of a three-phase voltage source through a three-phase load connected by a star with a harmonic suppression method. The output waveform and total harmonic distortion are measured using a digital storage oscilloscope and a harmonic analyzer. The content of the higher harmonics for each key management method is shown in Figures 14 to 16. Figure 14 shows the results of the for the at 120° -discrete switching method. Figure 15 shows the results of the fast Fourier transform for an inverter with a three-phase voltage source with 180° - discrete switching. Figure 16 shows a results of the fast Fourier transform for a three-phase voltage with 150° discrete switching. Table 5 shows the comparison results of the discrete switching method for the inverter with a three-phase voltage source and the selective harmonic suppression method for the inverter with a three-phase voltage source for different switching methods.

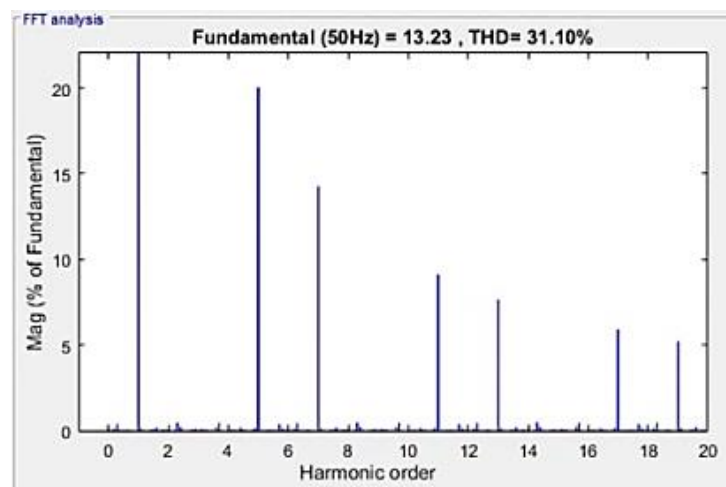


Figure 14. Fourier transformation results for 120° discrete switching

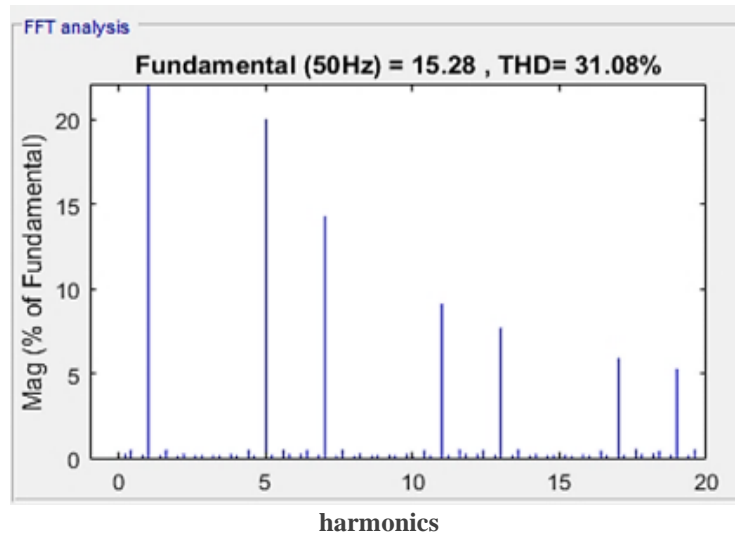


Figure 15. Fourier transformation results for 180° discrete switching

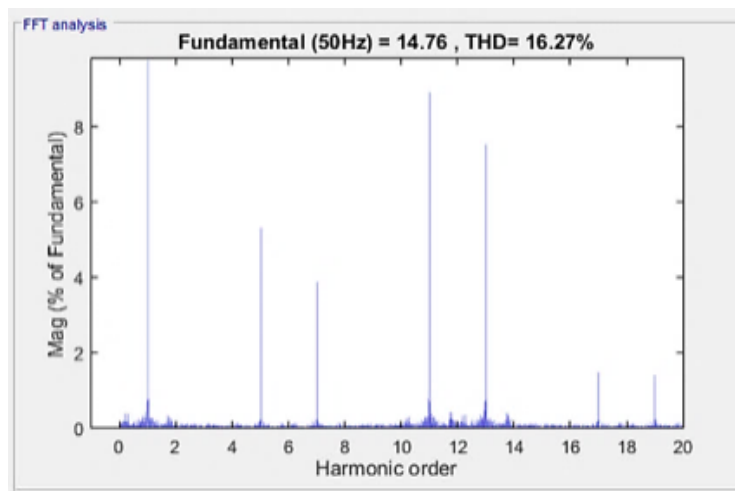


Figure 16. Fourier transformation results for 150° discrete switching

Table 5. Comparison of results

No.	Parameter	Switching method		
		120°	150°	180°
1	Hz	50	50	50
2	kV	0.954	0.979	0.955

4. CONCLUSION

Using semiconductor converters for the simulation of unbalanced (active and active-inductive) loads, models of a voltage balancing device based on a PI regulator and a relay regulator - P were developed in the MATLAB/Simulink environment. The simulation results showed the effectiveness of the proposed models under conditions of isolated sources of electrical energy. To describe the model, mathematical expressions are proposed describing voltage transformations under active-inductive load to establish changes in the degree of voltage symmetry under asymmetric loads. To evaluate the effectiveness of the proposed models, the harmonic spectrum was calculated by transforming the Fourier series. The harmonic spectrum results showed can be seen that the 150° discrete switching method is better than 120° and 180° discrete switching in terms of the magnitude of the ratio of the effective value of the first harmonic to the effective value of the total output voltage (kV).

ACKNOWLEDGMENT

The reported study was supported by Russian Science Foundation, research project No. 23-79-01024.





REFERENCES

- [1] M. Sadiq *et al.*, “Continuous-control-set model predictive control for three-level DC–DC converter with unbalanced loads in bipolar electric vehicle charging stations,” *Mathematics*, vol. 10, no. 19, Sep. 2022, doi: 10.3390/math10193444.
- [2] A. Ghulomzoda *et al.*, “A novel approach of synchronization of microgrid with a power system of limited capacity,” *Sustainability*, vol. 13, no. 24, p. 13975, Dec. 2021, doi: 10.3390/su132413975.
- [3] C. Guo, Y. Wang, and J. Liao, “Coordinated control of voltage balancers for the regulation of unbalanced voltage in a multi-node bipolar DC distribution network,” *Electronics*, vol. 11, no. 1, Jan. 2022, doi: 10.3390/electronics11010166.
- [4] S. S. Tavarov, I. Zicmane, S. Beryozkina, S. Praveenkumar, M. Safaraliev, and S. Shonazarova, “Evaluation of the operating modes of the urban electric networks in Dushanbe City, Tajikistan,” *Inventions*, vol. 7, no. 4, p. 107, Nov. 2022, doi: 10.3390/inventions7040107.
- [5] R. Pandey, R. N. Tripathi, and T. Hanamoto, “Comprehensive analysis of LCL filter interfaced cascaded H-bridge multilevel inverter-based DSTATCOM,” *Energies*, vol. 10, no. 3, Mar. 2017, doi: 10.3390/en10030346.
- [6] S. Hussain, A. Bakeer, I. S. Mohamed, M. Marchesoni, and L. Vaccaro, “Comparative study of passivity, model predictive, and passivity-based model predictive controllers in uninterruptible power supply applications,” *Energies*, vol. 16, no. 15, Jul. 2023, doi: 10.3390/en16155594.
- [7] S. S. Tavarov, P. Matrenin, M. Safaraliev, M. Senyuk, S. Beryozkina, and I. Zicmane, “Forecasting of electricity consumption by household consumers using fuzzy logic based on the development plan of the power system of the Republic of Tajikistan,” *Sustainability*, vol. 15, no. 4, p. 3725, Feb. 2023, doi: 10.3390/su15043725.
- [8] Z. Tang, Y. Yang, and F. Blaabjerg, “Loss unbalance issue of the full-bridge inverter with reactive power injection,” in *Conference Proceedings - IEEE Applied Power Electronics Conference and Exposition - APEC*, Jun. 2021, pp. 1451–1455, doi: 10.1109/APEC42165.2021.9487266.
- [9] J. Xu *et al.*, “A carrier-based two-phase-clamped DPWM strategy with zero-sequence voltage injection for three-phase quasi-two-stage buck-type rectifiers,” *IEEE Transactions on Power Electronics*, vol. 37, no. 5, pp. 5196–5211, May 2022, doi: 10.1109/TPEL.2021.3130677.
- [10] S. S. Tavarov *et al.*, “Control of operational modes of an urban distribution grid under conditions of uncertainty,” *Energies*, vol. 16, no. 8, Apr. 2023, doi: 10.3390/en16083497.
- [11] B. S. Gehrke, C. B. Jacobina, R. P. R. De Sousa, I. R. F. M. P. Da Silva, N. B. De Freitas, and M. B. D. R. Correa, “Single-phase three-wire power converters based on two-level and three-level legs using a space-vector PWM-based voltage balancing,” *IEEE Transactions on Industry Applications*, vol. 57, no. 3, pp. 2654–2665, May 2021, doi: 10.1109/TIA.2021.3063075.
- [12] Z. He *et al.*, “Optimized modulation method for three-level boost converter with ZVS under unbalanced-load operation,” *IEEE Transactions on Power Electronics*, vol. 38, no. 11, pp. 13811–13824, Nov. 2023, doi: 10.1109/TPEL.2023.3304300.
- [13] M. Asanov, S. Kokin, S. Asanova, K. Satarkulov, S. Dmitriev, and M. Safaraliev, “The use of Petri computing networks for optimization of the structure of distribution networks to minimize power losses,” *Energy Reports*, vol. 6, pp. 1337–1343, Dec. 2020, doi: 10.1016/j.egy.2020.11.024.
- [14] S. Dzhuraev *et al.*, “Computation of the zero-wire current under an asymmetric nonlinear load in a distribution network,” *Energy Reports*, vol. 8, pp. 563–573, Nov. 2022, doi: 10.1016/j.egy.2022.09.176.
- [15] O. Diene, C. F. Nascimento, E. H. Watanabe, L. G. B. Rolim, and A. G. P. Alves, “Analysis of grid-connected three-phase three-wire voltage-source converters operating with unbalanced conditions,” *Journal of Control, Automation and Electrical Systems*, vol. 35, no. 1, pp. 92–104, Nov. 2024, doi: 10.1007/s40313-023-01048-8.
- [16] Q. Wang, P. Yu, and P. Wang, “Resilience analysis and optimal control of grid-connected converters under unbalanced voltage conditions,” *IET Power Electronics*, vol. 16, no. 11, pp. 1765–1775, Jul. 2023, doi: 10.1049/pe12.12262.
- [17] Q. Chen, C. Klumpner, and M. R. Ahmed, “An unbalanced capacitor voltage buck converter with wide soft switching range,” *IEEE Transactions on Industrial Electronics*, vol. 71, no. 8, pp. 8703–8713, Aug. 2024, doi: 10.1109/TIE.2023.3314856.
- [18] A. Moradi, J. Yaghoobi, F. Zare, and D. Kumar, “Analysis of 0–9 kHz current harmonics in a three-phase power converter under unbalanced-load conditions,” *IEEE Access*, vol. 9, pp. 161862–161876, 2021, doi: 10.1109/ACCESS.2021.3131304.
- [19] C. Roh, “Optimal selection among various three-phase four-wire back-to-back (BTB) converters with comparative analysis for wave energy converters,” *Processes*, vol. 11, no. 5, May 2023, doi: 10.3390/pr11051463.
- [20] B. S. Naik, R. P. Reddy, S. Shan, L. Umanand, K. Gopakumar, and R. B. Subba, “A novel least component count single DC-link fed generalized multilevel inverter configuration for three-phase high power isolated grid connected systems,” in *2018 IEEE Energy Conversion Congress and Exposition (ECCE)*, Sep. 2018, pp. 2976–2981, doi: 10.1109/ECCE.2018.8557662.
- [21] B. Zhu *et al.*, “AC voltage synthesis using arbitrary two-phase voltages: Frequency, phase, and amplitude modulation for direct AC-AC power conversion,” *IEEE Transactions on Power Electronics*, vol. 37, no. 10, pp. 11855–11864, Oct. 2022, doi: 10.1109/TPEL.2022.3176398.
- [22] M. Antivachis, J. A. Anderson, D. Bortis, and J. W. Kolar, “Analysis of a synergetically controlled two-stage three-phase DC/AC buck-boost converter,” *CPSS Transactions on Power Electronics and Applications*, vol. 5, no. 1, pp. 34–53, Mar. 2020, doi: 10.24295/CPSSPEA.2020.00004.
- [23] A. W. S. Ramalho, M. A. Vitorino, M. B. D. R. Correa, L. A. L. D. A. C. Costa, and E. R. Braga-Filho, “New family of two-to-three-phase AC-AC indirect matrix converters with open-end rectifier stage,” *IEEE Transactions on Industry Applications*, vol. 58, no. 1, pp. 517–530, Jan. 2022, doi: 10.1109/TIA.2021.3128369.
- [24] A. H. Elmeligy, E. A. Gouda, and A. Elmitwally, “Design and implementation of a four-quadrant six-phase induction motor drive,” in *2022 23rd International Middle East Power Systems Conference (MEPCON)*, Dec. 2022, pp. 1–7, doi: 10.1109/MEPCON55441.2022.10021724.
- [25] B. Singh, Anuradha, D. P. Kothari, and A. Chandra, “Variable structure control of four pole voltage source inverter for active filtering of nonlinear loads in 3-phase 4-wire systems,” in *Power Quality '98*, 1998, pp. 89–94, doi: 10.1109/PQ.1998.710360.
- [26] K. H. Tan, F. J. Lin, and J. H. Chen, “A three-phase four-leg inverter-based active power filter for unbalanced current compensation using a petri probabilistic fuzzy neural network,” *Energies*, vol. 10, no. 12, Dec. 2017, doi: 10.3390/en10122005.
- [27] R. Aboelsaud, A. Ibrahim, and A. G. Garganeev, “Voltage control of autonomous power supply systems based on PID controller under unbalanced and nonlinear load conditions,” in *Proceedings of the 1st IEEE 2019 International Youth Conference on Radio Electronics, Electrical and Power Engineering, REEPE 2019*, Mar. 2019, pp. 1–6, doi: 10.1109/REEPE.2019.8708841.




- [28] P. Hsu and M. Behnke, "A three-phase synchronous frame controller for unbalanced load [inverter operation]," in *PESC 98 Record. 29th Annual IEEE Power Electronics Specialists Conference (Cat. No.98CH36196)*, 2002, vol. 2, pp. 1369–1374, doi: 10.1109/PESC.1998.703214.
- [29] M. Mokhtari, S. Golshannavaz, D. Nazarpour, and F. Aminifar, "Design of an asymmetrical three-phase inverter for load balancing and power factor correction based on power analysis," *Journal of Electrical Engineering and Technology*, vol. 6, no. 3, pp. 293–301, May 2011, doi: 10.5370/JEET.2011.6.3.293.
- [30] A. Ghulomzoda *et al.*, "Recloser-based decentralized control of the grid with distributed generation in the Lahsh district of the Rasht grid in Tajikistan, Central Asia," *Energies*, vol. 13, no. 14, pp. 1–18, Jul. 2020, doi: 10.3390/en13143673.
- [31] M. Azizur Rahman, "Analysis of current controllers for voltage-source inverter," *IEEE Transactions on Industrial Electronics*, vol. 44, no. 4, pp. 477–485, 1997, doi: 10.1109/41.605621.
- [32] M. P. Kazmierkowski and L. Malesani, "Current control techniques for three-phase voltage-source pwm converters: A survey," *IEEE Transactions on Industrial Electronics*, vol. 45, no. 5, pp. 691–703, 1998, doi: 10.1109/41.720325.
- [33] D. M. Brod and D. W. Novotny, "Current control of VSI-PWM inverters," *IEEE Transactions on Industry Applications*, vol. IA-21, no. 3, pp. 562–570, May 1985, doi: 10.1109/TIA.1985.349711.
- [34] L. Malesani and P. Tenti, "A novel hysteresis control method for current-controlled voltage-source PWM inverters with constant modulation frequency," *IEEE Transactions on Industry Applications*, vol. 26, no. 1, pp. 88–92, 1990, doi: 10.1109/28.52678.
- [35] S. Ogasawara, H. Akagi, and A. Nabae, "A novel PWM scheme of voltage source inverters based on space vector theory," *Archiv für Elektrotechnik*, vol. 74, no. 1, pp. 33–41, Jan. 1990, doi: 10.1007/BF01573229.
- [36] B. C. Babu, B. V. Reddy, and K. B. Mohanty, "A novel delta modulator and modified ramp type current controller-two viable scheme for current controlled voltage source inverter," *International Journal of Computer Applications*, vol. 1, no. 3, pp. 58–63, Feb. 2010, doi: 10.5120/84-182.
- [37] A. Nachiappan, K. Sundararajan, and V. Malarselvam, "Current controlled voltage source inverter using hysteresis controller and PI controller," in *2012 International Conference on Power, Signals, Controls and Computation, EPSCICON 2012*, Jan. 2012, pp. 1–6, doi: 10.1109/EPSCICON.2012.6175247.
- [38] A. Tripathi and P. C. Sen, "Comparative analysis of fixed and sinusoidal band hysteresis current controllers for voltage source inverters," *IEEE Transactions on Industrial Electronics*, vol. 39, no. 1, pp. 63–73, 1992, doi: 10.1109/41.121913.
- [39] A. Bashaireh, M. Mosa, R. S. Balog, and H. Abu-Rub, "Optimum number of cascaded multilevel inverters for high-voltage applications based on Pareto analysis," in *2017 IEEE Texas Power and Energy Conference (TPEC)*, Feb. 2017, pp. 1–6, doi: 10.1109/TPEC.2017.7868286.
- [40] N. Muruganatham and S. Palani, "Hybrid intelligent controllers based speed control of PMBLDC motor using soft-switching inverter," *International Journal of Electrical Engineering*, vol. 5, no. 7, pp. 863–880, 2012.
- [41] M. N. Uddin and M. A. Rahman, "Fuzzy logic based speed control of an IPM synchronous motor drive," in *Canadian Conference on Electrical and Computer Engineering*, 1999, vol. 3, pp. 1259–1264, doi: 10.1109/ccece.1999.804872.
- [42] S. K. Panda, X. M. Zhu, and P. K. Dash, "Fuzzy gain scheduled PI speed controller for switched reluctance motor drive," in *IECON Proceedings (Industrial Electronics Conference)*, 1997, vol. 3, pp. 989–994, doi: 10.1109/iecon.1997.668410.
- [43] M. Zerikat and S. Chekroun, "Design and implementation of a hybrid fuzzy controller for a high-performance induction," *International Journal of Computer and Information Engineering*, vol. 1, no. 2, 2007.
- [44] K. C. Ng, Y. Li, D. J. Murray-Smith, and K. C. Sharman, "Genetic algorithms applied to fuzzy sliding mode controller design," in *IEE Conference Publication*, 1995, vol. 1995, no. 414, pp. 220–225, doi: 10.1049/cp:19951052.
- [45] K. C. Ng and Y. Li, "Design of sophisticated fuzzy logic controllers using genetic algorithms," in *IEEE International Conference on Fuzzy Systems*, 1994, vol. 3, pp. 1708–1712, doi: 10.1109/fuzzy.1994.343598.
- [46] M. V. Aware, A. G. Kothari, and S. O. Choube, "Application of adaptive neuro-fuzzy controller (ANFIS) for voltage source inverter fed induction motor drive," in *Proceedings - IPEMC 2000: 3rd International Power Electronics and Motion Control Conference*, 2000, vol. 2, pp. 935–939, doi: 10.1109/IPEMC.2000.884638.
- [47] H. M. Soliman, "Improve the performance characteristics of induction motor through Bang Bang controller," *International Journal of Emerging Technology and Advanced Engineering*, vol. 6, no. 10, pp. 36–45, 2016.
- [48] P. K. Ainah, A. Muhammad, and G. Biwei, "DSP TMS320F28335 implementation of dq-PI vector controller for voltage source inverter using SPWM technique," *Nigerian Journal of Engineering*, vol. 27, no. August, pp. 106–112, 2020.
- [49] S. Swaroop, R. Kumar, A. Kumar, and N. Kumar, "Harmonic reduction in reduced power switch multilevel inverter using genetic optimization," in *2021 Asian Conference on Innovation in Technology (ASIANCON)*, Aug. 2021, pp. 1–7, doi: 10.1109/ASIANCON51346.2021.9544520.
- [50] Y. Deng and Q. Zhang, "Resonance overvoltage control algorithms in long cable frequency conversion drive based on discrete mathematics," *Open Physics*, vol. 18, no. 1, pp. 408–418, Aug. 2020, doi: 10.1515/phys-2020-0120.

BIOGRAPHIES OF AUTHORS






Saidjon Tavarov     received a degree in electrical engineering from the Tajik Technical University in 2008. In 2011 he received a Ph.D. in technical sciences from the South Ural State University. The area of scientific interests is the forecasting of power consumption, increasing the forecasting power consumption, improving reliability, energy efficiency. He can be contacted at email: tabarovsaid@mail.ru.






Mihail Senyuk    received the B.S., M.S., and Ph.D. degrees power engineering from Ural Federal University, Russia in 2016, 2018 and 2022, respectively. Currently, he is a senior researcher at the Department of Automated Electrical Systems Department, Ural Energy Institute, Ural Federal University, Yekaterinburg, Russia. His fields of interests include, power systems emergency control, power system transient and small signal stability, digital signal processing and machine learning. He can be contacted at email: mdsenuk@gmail.com.






Murodbek Safaraliev    received the B.S. and M.S. degrees electrical engineering from Tajik Technical University named after academic M. S. Osimi, Tajikistan, in 2014 and 2016, respectively, and Ph.D. degree in electrical power engineering from Ural Federal University, Russia in 2022. Currently, he is a senior researcher at the Department of Automated Electrical Systems Department, Ural Energy Institute, Ural Federal University, Yekaterinburg, Russia. His fields of interests include, optimization of the development, and modes of power system, planning of hybrid renewable energy systems. He can be contacted at email: murodbek_03@mail.ru.






Sergey Kokin    received a degree in electrical engineering in 1978 from the Ural Polytechnic Institute, and Ph.D. and Dr.sc.en degree in electrical power engineering from Ural Federal University, Russia in 1984 and 2013 respectively. Currently, he is a professor at the Department of Automated Electrical Systems, Ural Energy Institute, Ural Federal University, Yekaterinburg, Russia. His fields of interests include, model of the development, and modes of power system, planning of energy systems. He can be contacted at email: s.e.kokin@urfu.ru.



Alexander Tavlintsev    received the B.Sc. (2008), M.Sc. (2010) and Ph.D. (2018) in electrical engineering. Since 2010 he is employed by the Ural Energy Institute of Ural Federal University. Now he works as lecture and researcher. His research interests include data statistical analysis of electrical power systems. Automated Electric Systems Department Ural Federal University, Yekaterinburg, Russia. He can be contacted at email: a.s.tavlintsev@urfu.ru.



Andrey Svyatykh    Ph.D., First Deputy General Director of Uralenergosbyt LLC, defended his Ph.D., thesis in 2010. Research interests - control of the technical condition of liquid insulation of oil-filled high-voltage electrical equipment. He can be contacted at email: svyatykh@mail.ru.